Am J Cancer Res 2017;7(9):1948-1958
www.ajcr.us /ISSN:2156-6976/ajcr0060576

Original Article

Post-translationally modified muscle-specific ubiquitin ligases as circulating biomarkers in experimental cancer cachexia

Roberto Mota[1,2], Jessica E Rodríguez[3,4], Andrea Bonetto[5,6,7,8], Thomas M O'Connell[6,7,8,9], Scott A Asher[9,10], Traci L Parry[1,3], Pamela Lockyer[1,3], Christopher R McCudden[3,11], Marion E Couch[6,7,9], Monte S Willis[1,3,12]

[1]McAllister Heart Institute, University of North Carolina, Chapel Hill, NC, USA; [2]Division of Vascular Surgery, Department of Surgery, University of North Carolina, Chapel Hill, NC, USA (Current); [3]Department of Pathology & Laboratory Medicine, University of North Carolina, Chapel Hill, NC, USA; [4]Montefiore Medical Center, The University Hospital for Albert Einstein College of Medicine, Bronx, NY, USA (Current); [5]Department of Surgery, Indiana University School of Medicine, Indianapolis, IN, USA; [6]Department of Otolaryngology, Head and Neck Surgery, Indiana University School of Medicine, Indianapolis, IN, USA; [7]Simon Cancer Center, Indiana University School of Medicine, Indiana University-Purdue University at Indianapolis, Center for Cachexia Research, Innovation and Therapy, Indiana University School of Medicine, Indianapolis, IN, USA; [8]Indiana Center for Musculoskeletal Health, Indiana University, Indianapolis, IN, USA; [9]Department of Otolaryngology-Head and Neck Surgery, University of North Carolina, School of Medicine, Chapel Hill, North Carolina, USA; [10]Division of Surgery, Department of Clinical Sciences, The Florida State University College of Medicine, Tallahassee, FL, USA (Current); [11]Department of Pathology & Laboratory Medicine, University of Ottawa, Ottawa ON, Canada (Current); [12]Department of Pharmacology, University of North Carolina, Chapel Hill, NC, USA

Received June 30, 2017; Accepted August 24, 2017; Epub September 1, 2017; Published September 15, 2017

Abstract: Cancer cachexia is a severe wasting syndrome characterized by the progressive loss of lean body mass and systemic inflammation. Up to 80% of cancer patients experience cachexia, with 20-30% of cancer-related deaths directly linked to cachexia. Despite efforts to identify early cachexia and cancer relapse, clinically useful markers are lacking. Recently, we identified the role of muscle-specific ubiquitin ligases Atrogin-1 (MAFbx, FBXO32) and Muscle Ring Finger-1 in the pathogenesis of cardiac atrophy and hypertrophy. We hypothesized that during cachexia, the Atrogin-1 and MuRF1 ubiquitin ligases are released from muscle and migrate to the circulation where they could be detected and serve as a cachexia biomarker. To test this, we induced cachexia in mice using the C26 adenocarcinoma cells or vehicle (control). Body weight, tumor volume, and food consumption were measured from inoculation until ~day 14 to document cachexia. Western blot analysis of serum identified the presence of Atrogin-1 and MuRF1 with unique post-translational modifications consistent with mono- and poly- ubiquitination of Atrogin-1 and MuRF1 found only in cachectic serum. These findings suggest that both increased Atrogin-1 and the presence of unique post-translational modifications may serve as a surrogate marker specific for cachexia.

Keywords: Cancer cachexia, biomarkers, muscle ring Finger-1, Atrogin-1, TRIM63, FBXO32

Introduction

Cancer cachexia is a common finding in patients with cancer, experienced as a marked unintended weight loss, sarcopenia, anorexia, and fatigue [1]. The metabolic changes are distinct from starvation, reduced caloric intake, or tumor alone [2]. It's estimated that ~1.5 million people in the United States experience cancer cachexia each year, with those resulting from gastrointestinal, head and neck, lung, and prostate solid tumors most affected by cachexia (as recently reviewed) [1]. Cachexia is often an early finding in cancer and cancer recurrence, with detrimental effects on a patient's function, quality of life (QOL) measures, and has consequences such as immobility and cardiac/respiratory failure [3, 4]. The common clinical findings of cachexia include anorexia or reduced nutritional intake, a systemic inflammatory response, decreased muscle strength and fatigue [5, 6]. In addition to these three findings, biochemical alterations such as anemia, evidence of ongoing inflammatory response,

and low albumin have been proposed as markers [7]. However, these criteria and biochemical markers lack sensitivity and specificity and do not generally identify cachexia until later in the pathophysiology of the disease, when physical symptoms can be obvious.

Recently, the molecular mechanisms underlying skeletal muscle and cardiac atrophy have begun to be elucidated. As early as 1997, the role of the ubiquitin proteasome system in muscle atrophy was evident, with proteasome inhibition reducing the experimental skeletal muscle atrophy [8]. Later, identification of two muscle-specific ubiquitin ligases (E3s) play an important role in understanding the molecular mechanisms of skeletal muscle atrophy [9] and later cardiac atrophy [10]. These initial studies demonstrated that the lack of these E3s (MuRF1 and Atrogin-1) could significantly prevent muscle atrophy [9, 10]. After three days of unilateral lower limb suspension and limb immobilization, increases in Atrogin-1 and MuRF1 were identified in human biopsies [11]. Similarly, after immobilization in humans leads to increases in skeletal muscle Atrogin-1 and MuRF1 [12]. In humans receiving an LVAD (left ventricular assist device) to unload the heart as a bridge to transplant, elevations in both Atrogin 1 [13] and MuRF1 [10] have been identified.

Recent studies have identified the presence of circulating muscle-specific Atrogin-1 and MuRF1 by ELISA in both rats and humans [14]. In the present study, we sought to determine the character and quantity of circulating Atrogin-1 and MuRF1 using an established cancer mouse model from two independent laboratories as a possibly novel biomarker of cachexia.

Materials and methods

Animals, cachexia model, and human studies

Eight-week-old BALB/c mice (Charles River Laboratories (Wilmington, MA) and CD2F1 mice (Harlan Laboratories, Indianapolis, IN) were obtained and acclimated for a minimum of 10 days. Cohort 1 (Serum collected): Cancer cachexia was induced in BALB/c mice by subcutaneous (s.c.) injection of 0.5×10^6 C26 adenocarcinoma cells (or PBS vehicle control) in the right flank in 100 microL sterile PBS (Cohort 1, N=3 Control, N=6 Experimental biological replicates). Cohort 2 (platelet-poor plasma collected): Cancer cachexia was induced in CD2F1 mice (n=5) by s.c. injection of 1×10^6 C26 adenocarcinoma cells intrascapularly (or saline vehicle control). Mice were bled prior to euthanasia on Day 17 by retro-orbital bleeding (Cohort 1) and Day 14 (Cohort 2) by cardiac puncture, as previously described [15-17]. Tumor volume measurements, body weight and food/water intake were assessed weekly until last time point, as previously described [15, 18]. All mouse experiments, housing, and euthanasia were approved by the Institutional Animal Care and Use Committees (IACUC) review boards at the University of North Carolina (Cohort 1) and Indiana University (Cohort 2) and complied with National Institutes of Health Guidelines for Use and care of Laboratory Animals and with the ethical standards laid down in the 1964 Declaration of Helsinki and its later amendments. Use of the human plasma used in this study was approved by the University of North Carolina Institution Review Board (No. 05-2659; formerly 05-SURG-1224-ORC) and collected on Oncology protocol LCCC 0612 (Metabolomic analysis of cachexia in head and neck cancer patients). Use of the human heart tissue used in this study was approved by the University of North Carolina Institution Review Board (No. 03-1359).

Serum, plasma, and platelet-poor plasma (PPP) collection

Mouse serum: On Day 17 just prior to euthanasia ~200 microliters of whole blood was collected via retro orbital bleed directly into pediatric serum separator tubes with clot activator (Cat.#367983, Becton Dickinson and Co., Franklin Lakes, NJ). Blood was incubated at RT for 1 h, centrifuged for 10 minutes at 1300 × g, before serum was collected and immediately stored at -80°C. Mouse PPP: On Day 14, upon euthanasia, platelet-poor plasma (PPP) was prepared from blood collected by cardiac puncture and placed on ice in EDTA microtainers, followed by centrifugation at 1,000 × g for 15 min, removal of the plasma, and a second centrifugation at 10,000 × g for 10 min at 4°C, as previously described [19]. Mouse serum and mouse PPP stored at -80°C until analyzed by immunoblot. Human pooled serum and plasma were stored at 4°C until analyzed by immunoblot.

Immunoblot detection of circulating mouse Atrogin-1 and MuRF1

Diluted mouse serum samples (1:400 final dilution) were denatured in NuPAGE LDS Sample Buffer with reducing agent (Cat.#NP0007 and Cat.#NP0004, Thermofisher Scientific, Inc.) at 70°C for 10 min and resolved on a 4-12% NuPage Bis-Tris gradient gel (Cat.#NP0322, Thermofisher Scientific, Inc.) along with molecular weight standards (Cat.#10748-010, ThermoFisher, Inc., Waltham, MA) at 200V for 45 min, then transferred onto PVDF membrane in 20% MeOH MES run buffer with 200V for 120 min. An anti-Atrogin-1 (Cat.#sc-33782 H-300, Rabbit polyclonal 1:500 in 1% Milk, Santa Cruz Biotechnology, Inc., Dallas, TX) was incubated with the membrane for 1 hr at RT, washed 3X with TBST, then incubated with an HRP-conjugated anti-rabbit antibody (Cat.#-NA934, 1:4000 in 5% Milk, GE Healthcare Life Sciences, Pittsburg, PA). PVDF membranes were washed 4 times (10 min each) with TBST, developed using the ECL™ Plus (GE Healthcare; Pittsburgh, PA), then visualized by exposure to Amersham Hyperfilm ECL™ (GE Healthcare; Pittsburgh, PA) and developed using a Konica Medical Film Developer (Exposure time ~3 min, Cat.#SRX-101A, Konica Minolta Medical and Graphic Inc., Wayne, NJ). Film images were digitized with a ScanMaker 9800XL TMA 1600 (Cat.#MRS-3200A3, Microtek, Grove, IL), exported as 300 DPI TIFF files (pixels: 1084 width, 920 height), and inverted in Photoshop (CS6, Ver. 13.0 x64, Adobe, San Jose, CA) for densitometric analysis. Quantitative densitometric analysis of ECL images was performed using ImageJ 1.50 g software for Mac (for film-derived TIFF images, NIH, Bethesda, MD) [20]. Diluted mouse platelet-poor plasma samples (1:25) were denatured in NuPAGE LDS Sample Buffer with reducing agent (Cat.#NP0007 and Cat.#NP0004, Thermofisher Scientific, Inc.) at 65°C for 10 min and resolved in parallel with molecular weight standards (Cat.#LC5602, In-vitrogen, Carlsbad, CA) on a 4-12% gradient Bis-Tris gel (Cat.#NP0322, Thermofisher Scientific, Inc.) by applying 200 V for 35 min in MES SDS running buffer (Cat.#NP0002, Thermofisher Scientific, Inc.). Proteins were transferred from Bis-Tris gel onto PVDF using the NuPAGE transfer buffer (Cat.#NP0006, Thermofisher Scientific, Inc.) with 20% MeOH at 30 V for 66 min. The PVDF membrane was blocked for 1 hr at RT in 5% dry milk in TBS with 0.1% Tween-20 (TBST) prior to overnight immunoblot with anti-Atrogin-1 (Cat.#sc-33782 H-300, Rabbit polyclonal 1:500 in 1% Milk, Santa Cruz Biotechnology, Inc., Dallas, TX) or anti-MuRF1 (Cat.#sc-27642 C-20, Goat polyclonal 1:200 in 5% BSA, Santa Cruz Biotechnology, Inc., Dallas, TX) at 4°C. Membranes were washed 3 times (10 min each) in TBST, incubated a secondary HRP-labeled anti-rabbit (Cat.#A9169, 1:15,000 in 1% Milk, Sigma-Aldrich, St. Louis, MO) or HRP-labeled anti-goat (Cat.#A4174, 1:10,000 in 5% BSA, Sigma-Aldrich, St. Louis, MO) for 1 hr at RT, washed 4 times (10 min each) with TBST, and developed using the ECL + Plus Western Blotting system (Cat.#RPN2132, GE Healthcare Life Sciences, Pittsburg, PA). Immunoblot signal was visualized using an Ultra-Violet Products (UVP) BioSpectrum Imaging System™ (Cat.#81-0346-01 rev d, UVP, Ltd., Upland, CA) with VisionWorksLS Software (Version 8.5.15064.8534, UVP, Ltd.). Quantitative densitometric analysis of ECL images was performed using VisionWorks™ LS (for UVP-captured images, UVP, Ltd.) [21]. Diluted human plasma samples and pooled serum sample. 7.5 microliters of 1:400 human plasma and diluted pooled serum was run per lane in LDS with reducing 10X DTT. Samples were run on 12 well 4-12% gradient Bis-Tris gel and transferred onto PVDF, as described above. The membrane was blocked in 5% milk, then immunoblotted with either: 1) anti-MuRF1 (1:1000 in TBS-T overnight at 4°C, Novus Biologicals Ab, Cat.#nb100-2406, Novus Biologicals, LLC), followed by an anti-goat antibody (1:10,000 in 5% milk for 1 hr at room temperature, Cat.#sc-2768, Santa Cruz Biotechnology); or 2) anti-Atrogin-1 (1:500 in 1% milk in TBST overnight at 4°C, Cat.#sc-33782 H-300, Santa Cruz Biotechnologies), followed by an anti-rabbit 1:4,000 (5% milk for 1 hr at room temperature, Cat#NA934, Amersham Biosciences, GE Healthcare). The human pooled serum was also assayed for CHIP using goat anti-CHIP (Millipore, cat.no. AB10000), followed by an anti-goat antibody (Cat.#sc-2768, Santa Cruz Biotechnology) and included human heart lysates controls loaded 10-50 micrograms per lane.

Statistical analyses

All data were subject to statistical analysis performed using two-tailed Student's t-test, with significance defined as $p<0.05$. All results are presented as the mean ± SEM. Data was ana-

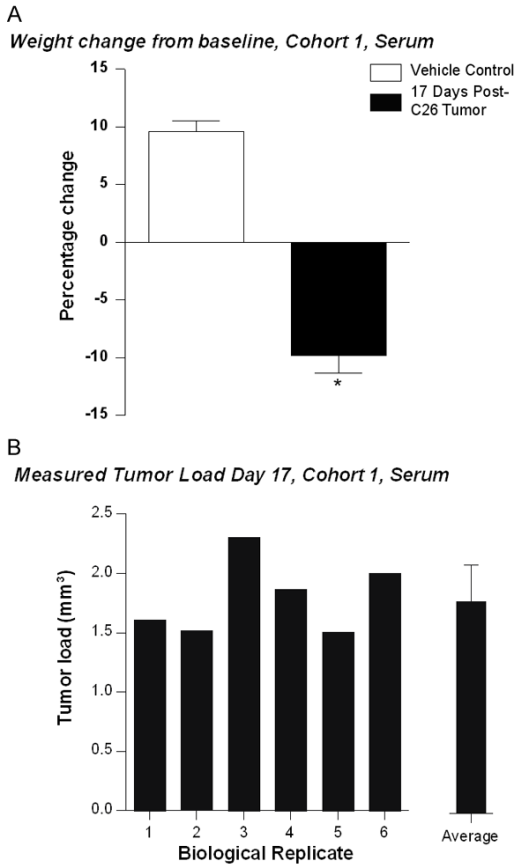

Figure 1. C26 tumor cell implantation cachectic model characterization. A. Percentage weight change (loss or gain) from baseline after 17 days comparing vehicle control treated mice and C26 tumor implanted mice (cachectic). A two-tailed Student's t-test was performed to determine significance. B. Tumor load measurement post-17 days of vehicle (saline) or C26 tumor implantation. Each bar in the left graph represents a mouse sample; the adjacent graph on the right represents the mean ± SEM. N=3 (vehicle controls), N=6 (C26 adenocarcinoma treated). *p<0.0001.

lyzed using Microsoft Excel for Mac 2011 (Version 14.6.3, Redmond, WA) and Prism for Mac (Version 7.0, GraphPad, Inc., San Diego, CA) for all analyses performed.

Results

Two independent mouse models of cachexia were studied here using the C26 carcinoma cancer cachexia model. In the first, 0.5×10^6 C26 carcinoma cells were injected subcutaneously (s.c.) into the right flank of BALB/c mice, where the tumors developed until day 17, when we collected serum. In the second model, 10^6 C26 carcinoma cells were injected s.c. between their scapula, where tumors developed until day 14, when platelet-poor plasma was collected. The collected serum and plasma were then analyzed by immunoblot analysis for the presence of the muscle-specific ubiquitin ligases Atrogin-1 and MuRF1, as a potential biomarker of muscle involvement in cachexia. In BALB/c mice with tumor growth for 17 days, a significant decrease was identified in mice with C26 tumors, with an average of weight loss from baseline of 9.8 g ($p<0.0001$) (**Figure 1A**). In contrast, vehicle-treated controls gained nearly 10% from their starting weights, illustrating a 15-20% difference in body weight in mice with the C26 carcinoma, consistent with cachexia as previously reported [15, 18, 22]. In each of the six biological replicates, tumor load at harvest by measurement averaged 1.8 mm [3] (**Figure 1B**, Supplemental Figure 1A). No changes in food or water intake were noted over the 17 day experiment, as previously reported [15, 18, 22].

Western analysis of diluted serum identified both qualitative and quantitative changes in circulating Atrogin-1 (**Figure 2A**). Vehicle control animals had circulating Atrogin-1 present, as indicated by the black arrow in the 50 + kDa MW range (**Figure 2A**). This finding was surprising since ubiquitin ligases have not been described as routine circulating proteins to our knowledge in the healthy state. In contrast, Day 17 cachexia serum exhibited a consistent higher molecular weight band not seen in the healthy animals, indicated by the blue arrow (**Figure 2A**). Similarly, higher molecular weight bands were seen prominently in 4 of the 6 samples, including increased levels of molecular weight bands in the 180 + kDa range, highlighted by red lines to the right of the six lanes (**Figure 2A**). Densitometric analysis of each of samples identified a significant increased ($p<0.05$) in Atrogin-1 and its apparent higher molecular bands (>2 fold) were present in mice with cachexia (**Figure 2B**). These additional higher molecular weight Atrogin-1 species made up most of the increase in serum Atrogin-1 seen in day 17 cachectic mice.

When CDF1 mice were challenged with C26 carcinoma cells for 14 days, significant decreases in final body weight, gastrocnemius weigh, quadriceps, heart, and fat were significantly decreased (**Figure 3A**, Supplemental Figure 1B). Western analysis of diluted platelet-poor plasma (PPP) revealed the 50 + kDa MW

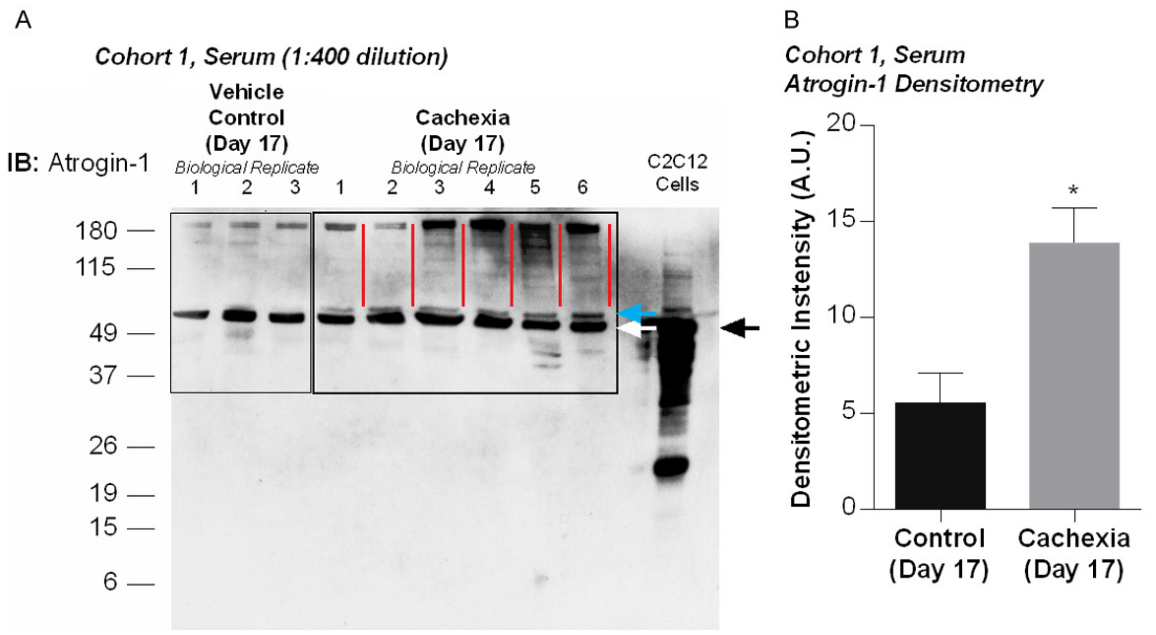

Figure 2. Western blot analysis of serum Atrogin-1 in experimental cohort 1. A. Serum (1:400 diluted samples) from control treated mice (N=3) and C26 tumor bearing mice (cachectic) (N=6), ran with a parallel C2C12 lysate control. Bars in red offset the post-translational modifications of Atrogin-1. *White arrow:* expected molecular weight band for Atrogin-1. *Blue arrow:* represents the smallest post-translational modification identified. *Red bar:* highlights the higher molecular weight post-translational modifications identified. *Black arrow:* indicates the expected molecular weight of Atrogin-1 in C2C12 cell lysates. B. Densitometric analysis of Atrogin-1 identified significant increases in immunoreactive Atrogin-1 (all molecular weight species) in cachexia mouse serum compared to controls. A two-tailed Student's t-test was performed to determine significance. *p<0.05.

Atrogin-1 band, indicated by a black arrow in **Figure 3B**, seen in the serum cohort (**Figure 2A**). Unique higher molecular band species were seen in the cachexia serum samples at day 14, indicated by the blue arrow (**Figure 3B**), along with increases in higher molecular bands indicated by the blue bars (**Figure 3B**). Smaller molecular weight Atrogin-1 reactive bands were also seen uniquely in the cachexia serum at 14 days, indicated by the red arrow (**Figure 3B**). As similarly found in our first experimental group, the density of all the Atrogin-1 bands was significantly increased and >2 fold higher in the cachexia serum, compared to vehicle-treated controls (**Figure 3C**).

In separate analyses of MuRF1 in CD2F1 PPP, alterations in circulating MuRF1 levels were identified (**Figure 3D**). Vehicle-treated mouse plasma appears to have MuRF1 reactive protein species, indicated by the black arrow in **Figure 3D.** Serum from cachectic mice illustrated unique higher molecular specifies (blue arrow, **Figure 3D**) and lower molecular species (red arrow, **Figure 3D**), in addition to increased amounts of immunoreactive MuRF1 proteins of higher and low molecular weights shown by blue and red lines to the left of the lanes (**Figure 3D**). Densitometric analysis of MuRF1 demonstrated that cachectic mice had approximately three times the overall immunoreactive MuRF1 compared to vehicle controls (**Figure 3E**). Using the reagents that detected Atrogin-1 and MuRF1 in mouse serum and platelet poor plasma, both Atrogin-1 and MuRF1 were recognized by immunoblot in human plasma and serum samples in the current study (Supplemental Figures 2A, 2B, 3A, 3B). In four biological controls, human plasma analyzed by immunoblot for Atrogin-1 revealed a 55 kDa band (Supplemental Figure 2A), paralleling the protein identified in mice (**Figure 2A**). Similarly, human plasma analyzed for MuRF1 revealed a single band aligning with the human heart control run in the far lane (Supplemental Figure 2B), paralleling that found in control mice (**Figure 3D**). Immunoblot analysis of Atrogin-1 and MuRF1 in serial dilutions of human pooled serum detected Atrogin-1 (Supplemental Figure 3A) and MuRF1 (Supplemental Figure 3B) at the predicted molecular weights, corresponding to that found in human heart lysates ran in

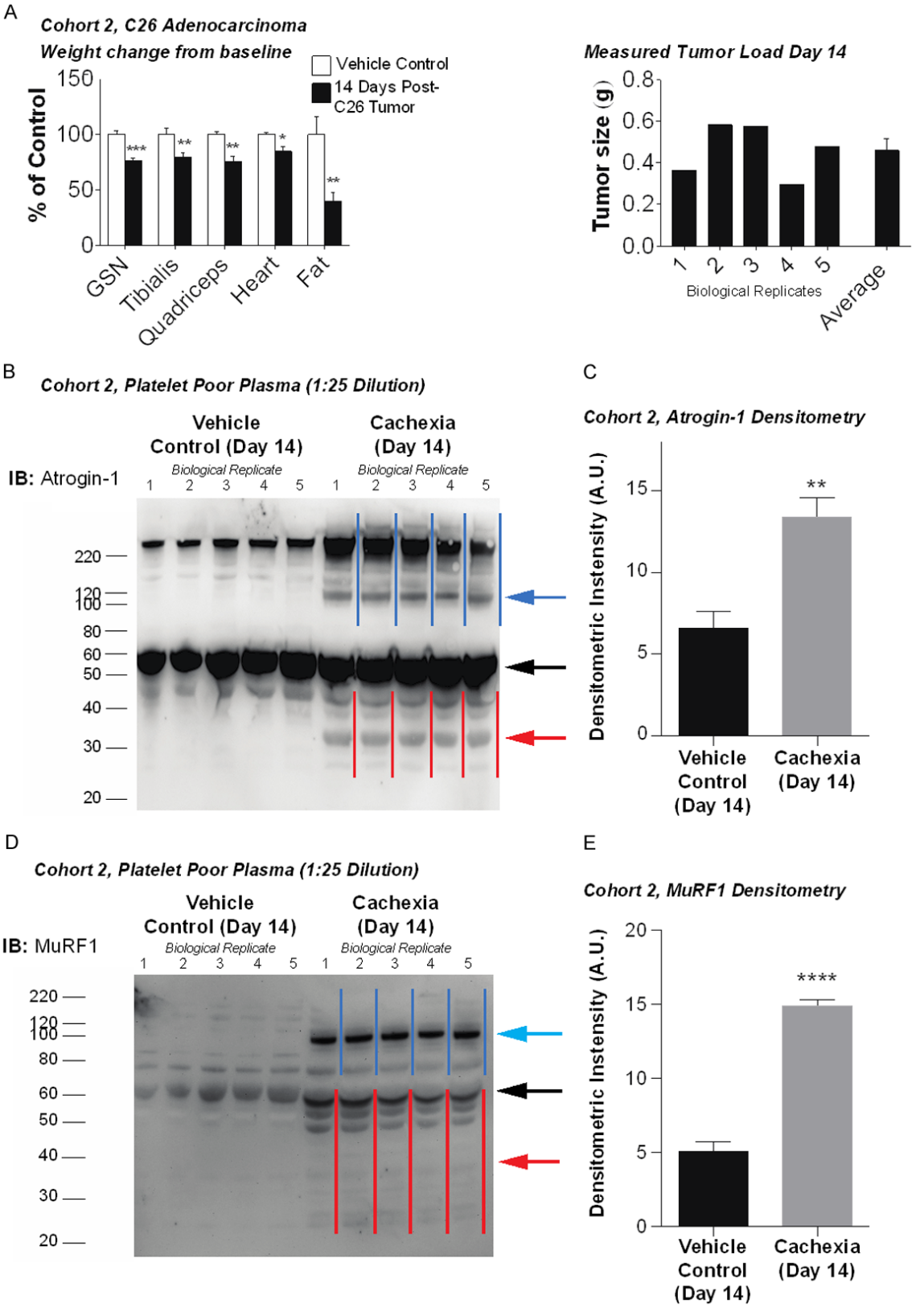

Figure 3. Western blot analysis of platelet poor plasma Atrogin-1 and MuRF1 in experimental cohort 2. (A) Changes in muscle groups (gastrocnemius (GSN), tibialis anterior, quadriceps, heart, and fat) 14 days after C26 tumor implantation (top left). The average tumor load of the tumor treated mice was approximately 0.5 g (top right). (B) Immunoblot analysis of platelet poor plasma samples (1:400 dilution) C26 tumor bearing (cachectic) (N=6) and

control mice (N=3), along with a mouse heart lysate positive control. (C) Densitometric analysis of (B). (D) Immunoblot analysis of platelet poor plasma (1:25 dilution) from C26 tumor bearing (cachectic) (N=5) and control mice (N=5) and were ran with mouse heart lysate control. (E) Densitometric analysis of (D). The region of interest in each lane of (B and D) was performed using the rectangular image tool, with plots constructed representing peak intensity in each lane, as previously described [20]. *Blue arrow/blue bar:* postulated post-translational modifications of Atrogin-1 (B) or MuRF1 (D). *Black arrow:* expected molecular weight band for Atrogin-1 (B) or MuRF1 (D). *Red arrow/red bar:* indicates the postulated degradation products of Atrogin-1 (B) or MuRF1 (D). Densitometric analysis was performed on each lane and included the multiple molecular weight species (indicated by the blue, black, and red arrows). The densitometric values of each of these species were then added together (grouped) and statistically analyzed to compare the cachexia vs control groups. *p<0.05, **p<0.01, ***p<0.001, ****p<0.0001.

parallel controls. Lastly, identification of the ubiquitously expressed carboxy terminus of HSP-70 interacting protein (CHIP), encoded by the Stub1 gene, was found to be present in human serum (Supplemental Figure 2C). A complete chemistry profile of the pooled serum analyzed is found in Supplemental Table 1.

Discussion

The ubiquitin ligases Atrogin-1 and MuRF1 are found specifically in striated muscle [9] and were first recognized for their mechanistic roles in skeletal muscle atrophy in 2001 [9]. The presence of circulating Atrogin-1 and MuRF1 in "healthy" blood has not previously been reported, although they have been identified by ELISA to acute increase after myocardial infarction [14]. In these elegant studies, Atrogin-1 and MuRF1, along with 4 other cardiac and muscle-enriched ubiquitin ligases (Rnf207, MuRF3, Kbtbd10/KLHL41, Asb11, and Asb2) were investigated in acute myocardial infarction patients (AMI) [14]. Of these, Atrogin-1, MuRF1, Rnf207, Kbtbd10/KLHL41 were significantly increased compared to control animals after experimental acute myocardial infarction in rats [14]. In human acute myocardial infarction patients, Atrogin-1 and MuRF1 were found to increase by 1 hour, peak at 3 hours, and decrease at 6-24 hours, paralleling circulating levels these investigators identified in experimental rat surgically given an AMI [14]. Among the six E3s studied, the receiver operator curve (ROS) of the Ring Finger Protein 207 (RNF207) most closely compared to Troponin I sensitivity and specificity [14]. These studies were important for their identification of circulating Atrogin-1 and MuRF1 prior to AMI since they had not previously been identified. Notably, the investigators used ELISAs to identify the levels of circulating E3s, so any changes in molecular size (e.g., post-translational modifications) were not identifiable by ELISA, as they were in the present study. Other components of the ubiquitin proteasome system have been found circulating, which are distinct from the 20S proteasomes found in circulating blood cells [23], making it possible that circulating ubiquitin ligases have previously unidentified functions in their circulating forms.

The present study identified quantitative changes in the mouse of circulating immunoreactive Atrogin-1 and MuRF1 in the the C26 carcinoma tumor-bearing mouse model of cancer cachexia at 14 + days post-implantation [15, 17, 18, 24]. The study confirmed previously findings that Atrogin-1 and MuRF1 circulates in the healthy state [14], presumably from the routine turnover of muscle, as seen with circulating creatine kinase isoforms [25, 26]. However, the reason for the increased levels of proteins in not clear, but presumed to be secondary to inflammatory-mediated damage to muscle. In cancer cachexia patients, elevated LDH levels from myocyte damage has been reported [27]. Therefore, increased quantities of circulating Atrogin-1 and MuRF1 may be due to myocyte damage and release. What is most intriguing about the findings in the present study are the qualitative changes in immunoreactive Atrogin-1 and MuRF1. Specifically, the high molecular weight species circulating with cachexia are reminiscent of the mono-ubiquitination both Atrogin-1 (**Figure 2A**, blue arrow), poly-ubiquitination of Atrogin-1 (**Figures 2A**, **3B**, blue lines). MuRF1 is well known to both mono- [28, 29] and poly-ubiquitinate different substrates [30]. Additionally, in cell culture, increased MuRF1 expression significantly enhanced autoubiquitination [29, 30], which has not been reported in vivo previously. Since MuRF1 forms dimers with itself [31]. it is possible that this autoubiquitination may be either a feedback loop or may allow communications between striated muscle and other organ compartments. The potential for other post-translational modifications beyond ubiquitin certainly

exists, and may give further insight into the pathophysiology of diseases, in future studies.

Not only was the identification of increased circulating Atrogin-1 and MuRF1 seen in cancer cachexia in the present study, we identified post-translationally modified Atrogin-1 and MuRF1. One potential mechanism of this may be auto-ubiquitination, which has been shown in vitro when MuRF1 expression is increased in vitro [32, 33]. Post-translational alterations in proteins are important biomarkers of disease in use today, including the diagnosis of diabetes control and rheumatoid arthritis [34-36]. In diabetes, elevated levels of glucose induces the non-enzymatic glycation of proteins, whereby glucose reacts with amine groups to form a stable ketoamine Amadori Product (advanced glycation endproducts or AGEs) [37]. Of the glycated species, hemoglobin was identified for its diagnostic utility due to the stability of the amine group added [38]. Elevated levels of higher molecular weight hemoglobin (A1C or glycated Hemoglobin) indicate poor long-term glucose control that cannot be detected otherwise. Similarly, identification of proteins and peptides post-translationally modified with citrulline (citrullinated) are found in rheumatoid arthritis. Citrullinated proteins were identified as autoantigens [39]. Diagnostically, they have been found to have the highest specificity and sensitivity in diagnosing RA, with high positive predictive value in joint destruction [40]. Post-translational modifications of such markers have helped both in understanding the underlying pathophysiology of disease and provide a useful window for disease detection and treatment [41]. The role of the higher molecular weight Atrogin-1 and MuRF1 may have both roles in the pathophysiology of the systemic cachexia disease processes and/or may have diagnostic utility in future studies as diagnostic tests of early cachexia are generally lacking.

Current diagnostic criteria for cachexia are largely present much later in the pathophysiology of disease, and include the presence of non-edematous weight loss >5% in <12 months in the presence of cancer, in addition to 3 of the following criteria: decreased muscle strength, fatigue, anorexia, low FFM indices, or abnormal biochemistry (increased CRP, anemia, or decreased albumin) [1]. There is little to no specificity of these biochemical markers, which may or may not be present with cachexia [1], illustrating the need for better specific markers. Since early detection and disease-specific staging determine the outcomes of the cachectic-state [42], better markers of disease are needed. The current use of biomarkers of anemia, inflammation, and low albumin have been proposed as markers, but do not generally identify cachexia until later in the pathophysiology of the disease, when physical symptoms can be obvious [7]. The occurrence/recurrence detection window is often overlooked but in patients undergoing cancer treatment, the earlier the detection, the more likely the possibility of impacting their prognosis [1, 43, 44].

We studied two cohorts in the present study, which included two different strain mouse strains, in addition to two methodologies of capturing the western blots. In cohort 1, mice were injected with 0.5×10^6 C26 adenocarcinoma cells, while cohort 2 mice were injected with 1.0×10^6 C26 adenocarcinoma cells. The two doses correspond to the rapidness of the cachexia, with both cohort 1 and cohort 2 losing ~10% weight loss, but on days 17 and 14, respectively. The differences in response may also be related to strain differences (BALB/c in cohort 1, CD2F1 in cohort 2) in addition to the differences in the doses given. The identification of MuRF1 in mouse serum on Day 17 in cohort 1 was performed with serum diluted 1:400 and the western ECL detected using x-ray film and up to overnight exposure (**Figure 2**). In contrast, MuRF1 was detected in plasma only when diluted less than 1:400 (1:25 dilution) to detect western ECL using a camera-based system (**Figure 3**). These differences are likely due to the length of exposure allowed in the camera vs. the x-ray film systems, or differences in interferences in plasma vs. serum when detecting circulating ubiquitin ligases in experimental models of cancer cachexia.

This is the first time the muscle-specific atrogin-1 and MuRF1 ubiquitin ligases (E3) have been resolved on gel electrophoresis (Supplemental Figures 2, 3A, 3B), illustrating the diversity of molecular species (i.e., molecular weight forms) present. In addition to Atrogin-1 and MuRF1, other ubiquitously expressed E3 proteins critical in protein quality control such as the protein CHIP are also circulating in normal serum (Supplemental Figure 3C), which has not been previously described to our knowledge. Given CHIP's role in diseases such as cerebel-

lar ataxia [45], cystic fibrosis [46-48], and cardiac disease [49], its use diagnostically as biomarkers may be warranted as it is for the Atrogin-1 and MuRF1 in cancer cachexia identified here.

Future studies applying these findings in human disease should keep in mind the time-dependent manner by which increased MuRF1 and Atrogin-1 species are found circulating in mice after the deliberate placement of tumor in the present study and objective measures of cachexia are present, including significant reductions in fat and lean body (muscle) mass by MRI body composition analysis [1, 15, 17, 18, 43]. The experimental design here did seek to identify the earliest time points that increases in MuRF1 and Atrogin-1 are detectable, which would be a critical point in investigating these markers in patients with suspected or established cachexia. This is a particularly challenging issue in studying human cachexia as detection of cachexia by MRI is not routinely performed and pragmatically is diagnosed at later time points where weight loss is visually detectable. The type of cancer and progression is also an important variable that will need to be taken into account when correlating these biomarkers with the progression and timing of disease occurrence/recurrence.

Acknowledgements

The authors wish to thank Dr. Catherine Hammett-Stabler for her tremendous assistance with obtaining and analyzing the pooled human serum for the analysis. We also thank Drs. Nancy Moss and Craig H. Selzman for the assistance with obtaining the human tissue lysate controls. The Jefferson-Pilot Corporation Fellowship in Academic Medicine (to M.W.), the NIH National Heart, Lung, and Blood Institute (R01HL104129 to M.W.), the NIH National Cancer Institute (R21CA190028 to A.B.) supported these studies.

Disclosure of conflict of interest

None.

Abbreviations

C26, C26-adenocarcinoma cell line; CHIP, carboxy terminus of HSP-70 interacting protein; E3, ubiquitin ligase; Fbx032, F-box protein 32, also known as MAFbx/Atrogin-1; MAFbx, muscle atrophy F-box, also known as Fbox032/Atrogin-1; MuRF1, muscle ring finger-1; Trim63, tripartite motif-containing 63, also known as MuRF1.

Address correspondence to: Dr. Monte S Willis, McAllister Heart Institute, University of North Carolina, 111 Mason Farm Road, MBRB 2340B. Chapel Hill, NC 27599, USA; Department of Pathology & Laboratory Medicine, University of North Carolina, 111 Mason Farm Road, MBRB 2340B. Chapel Hill, NC 27599, USA; Department of Pharmacology, University of North Carolina, 111 Mason Farm Road, MBRB 2340B. Chapel Hill, NC 27599, USA. Tel: 919-843-1938; Fax: 919-843-4585; E-mail: monte_willis@med.unc.edu

References

[1] Couch ME, Dittus K, Toth MJ, Willis MS, Guttridge DC, George JR, Barnes CA, Gourin CG, Der-Torossian H. Cancer cachexia update in head and neck cancer: definitions and diagnostic features. Head Neck 2015; 37: 594-604.

[2] Der-Torossian H, Asher SA, JH Winnike, Wysong A, Yin X. Cancer cachexia's metabolic signature in a murine model confirms a distinct entity. Metabolomics 2013; 9: 730-739 .

[3] Lucia S, Esposito M, Rossi Fanelli F. Muscaritoli M. Cancer cachexia: from molecular mechanisms to patient's care. Crit Rev Oncog 2012; 17: 315-321.

[4] Stewart GD, Skipworth RJ. Fearon KC. Cancer cachexia and fatigue. Clinical Medicine 2006; 6: 140-143.

[5] Fearon K, Strasser F, Anker SD, Bosaeus I, Bruera E. Definition and classification of cancer cachexia: an international consensus. Lancet Oncology 2011; 12: 489-495.

[6] Strasser, F. Diagnostic criteria of cachexia and their assessment: decreased muscle strength and fatigue. Curr Opin Clin Nutr Metab Care 2008; 11: 417-421.

[7] Evans WJ, Morley JE, Argilés J, Bales C, Baracos V, Guttridge D, Jatoi A, Kalantar-Zadeh K, Lochs H, Mantovani G, Marks D, Mitch WE, Muscaritoli M, Najand A, Ponikowski P, Rossi Fanelli F, Schambelan M, Schols A, Schuster M, Thomas D, Wolfe R, Anker SD. Cachexia: a new definition. Clin Nutr 2008; 27: 793-799.

[8] Tawa NE Jr, Odessey R. Goldberg AL. Inhibitors of the proteasome reduce the accelerated proteolysis in atrophying rat skeletal muscles. Journal of Clinical Investigation 1997; 100: 197-203.

[9] Bodine SC, Latres E, Baumhueter S, Lai VK, Nunez L, Clarke BA, Poueymirou WT, Panaro FJ, Na E, Dharmarajan K, Pan ZQ, Valenzuela DM,

DeChiara TM, Stitt TN, Yancopoulos GD, Glass DJ. Identification of ubiquitin ligases required for skeletal muscle atrophy. Science 2001; 294: 1704-1708.

[10] Willis MS, Rojas M, Li L, Selzman CH, Tang RH, Stansfield WE, Rodriguez JE, Glass DJ, Patterson C. Muscle ring finger 1 mediates cardiac atrophy in vivo. Am J Physiol Heart Circ Physiol 2009; 296: H997-H1006.

[11] Gustafsson T, Osterlund T, Flanagan JN, von Waldén F, Trappe TA, Linnehan RM, Tesch PA. Effects of 3 days unloading on molecular regulators of muscle size in humans. J Appl Physiol (1985) 2010; 109: 721-727.

[12] Abadi A, Glover EI, Isfort RJ, Raha S, Safdar A, Yasuda N, Kaczor JJ, Melov S, Hubbard A, Qu X, Phillips SM, Tarnopolsky M. Limb immobilization induces a coordinate down-regulation of mitochondrial and other metabolic pathways in men and women. PLoS One 2009; 4: e6518.

[13] Baskin KK, Rodriguez MR, Kansara S, Chen W, Carranza S, Frazier OH, Glass DJ, Taegtmeyer H. MAFbx/Atrogin-1 is required for atrophic remodeling of the unloaded heart. J Mol Cell Cardiol 2014; 72: 168-176.

[14] Han QY, Wang HX, Liu XH, Guo CX, Hua Q, Yu XH, Li N, Yang YZ, Du J, Xia YL, Li HH. Circulating E3 ligases are novel and sensitive biomarkers for diagnosis of acute myocardial infarction. Clin Sci (Lond) 2015; 128: 751-760.

[15] Wysong A, Couch M, Shadfar S, Li L, Rodriguez JE, Asher S, Yin X, Gore M, Baldwin A, Patterson C, Willis MS. NF-kappaB inhibition protects against tumor-induced cardiac atrophy in vivo. Am J Pathol 2011; 178: 1059-1068.

[16] Bonetto A, Penna F, Minero VG, Reffo P, Bonelli G, Baccino FM, Costelli P. Deacetylase inhibitors modulate the myostatin/follistatin axis without improving cachexia in tumor-bearing mice. Curr Cancer Drug Targets 2009; 9: 608-616.

[17] Bonetto A, Kays JK, Parker VA, Matthews RR, Barreto R, Puppa MJ, Kang KS, Carson JA, Guise TA, Mohammad KS, Robling AG, Couch ME, Koniaris LG, Zimmers TA. Differential bone loss in mouse Models of colon cancer cachexia. Front Physiol 2016; 7: 679.

[18] Shadfar S, Couch ME, McKinney KA, Weinstein LJ, Yin X, Rodríguez JE, Guttridge DC, Willis M. Oral resveratrol therapy inhibits cancer-induced skeletal muscle and cardiac atrophy in vivo. Nutr Cancer 2011; 63: 749-762.

[19] Pedroso FE, Spalding PB, Cheung MC, Yang R, Gutierrez JC, Bonetto A, Zhan R, Chan HL, Namias N, Koniaris LG, Zimmers TA. Inflammation, organomegaly, and muscle wasting despite hyperphagia in a mouse model of burn cachexia. J Cachexia Sarcopenia Muscle 2012; 3: 199-211.

[20] Liang W, Mason AJ, Lam JK. Western blot evaluation of siRNA delivery by pH-responsive peptides. Methods Mol Biol 2013; 986: 73-87.

[21] Estes B, Hsu YR, Tam LT, Sheng J, Stevens J, Haldankar R. Uncovering methods for the prevention of protein aggregation and improvement of product quality in a transient expression system. Biotechnol Prog 2015; 31: 258-267.

[22] Der-Torossian H, Wysong A, Shadfar S, Willis MS, McDunn J, Couch ME. Metabolic derangements in the gastrocnemius and the effect of compound a therapy in a murine model of cancer cachexia. J Cachexia Sarcopenia Muscle 2013; 4: 145-155.

[23] Zoeger A, Blau M, Egerer K, Feist E, Dahlmann B. Circulating proteasomes are functional and have a subtype pattern distinct from 20S proteasomes in major blood cells. Clin Chem 2006; 52: 2079-2086.

[24] Bonetto A, Rupert JE, Barreto R1, Zimmers TA2. The Colon-26 carcinoma tumor-bearing mouse as a model for the study of cancer cachexia. J Vis Exp 2016.

[25] Klein SM, Prantl L, Geis S, Felthaus O, Dolderer J, Anker AM, Zeitler K, Alt E, Vykoukal J. Circulating serum CK level vs. muscle impairment for in situ monitoring burden of disease in Mdx-mice. Clin Hemorheol Microcirc 2017; 65: 327-334.

[26] Koch AJ, Pereira R, Machado M. The creatine kinase response to resistance exercise. J Musculoskelet Neuronal Interact 2014; 14: 68-77.

[27] Bilir C, Engin H, Can M, Temi YB, Demirtas D. The prognostic role of inflammation and hormones in patients with metastatic cancer with cachexia. Med Oncol 2015; 32: 56.

[28] Wadosky KM, Berthiaume JM, Tang W, Zungu M, Portman MA, Gerdes AM, Willis MS. MuRF1 mono-ubiquitinates TRa to inhibit T3-induced cardiac hypertrophy in vivo. J Mol Endocrinol 2016; 56: 273-290.

[29] Rodríguez JE, Liao JY, He J, Schisler JC, Newgard CB, Drujan D5, Glass DJ, Frederick CB, Yoder BC, Lalush DS, Patterson C, Willis MS. The ubiquitin ligase MuRF1 regulates PPARalpha activity in the heart by enhancing nuclear export via monoubiquitination. Mol Cell Endocrinol 2015; 413: 36-48.

[30] Li HH, Du J, Fan YN, Zhang ML, Liu DP, Li L, Lockyer P, Kang EY, Patterson C, Willis MS. The ubiquitin ligase MuRF1 protects against cardiac ischemia/reperfusion injury by its proteasome-dependent degradation of phospho-c-Jun. Am J Pathol 2011; 178: 1043-1058.

[31] Witt SH, Granzier H, Witt CC, Labeit S. MURF-1 and MURF-2 target a specific subset of myofibrillar proteins redundantly: towards understanding MURF-dependent muscle ubiquitination. J Mol Biol 2005; 350: 713-722.

[32] Mattox TA, Young ME, Rubel CE, Spaniel C, Rodríguez JE, Grevengoed TJ, Gautel M, Xu Z, Anderson EJ, Willis MS. MuRF1 activity is present in cardiac mitochondria and regulates reactive oxygen species production in vivo. J Bioenerg Biomembr 2014; 46: 173-187.
[33] Bodine SC, Baehr LM. Skeletal muscle atrophy and the E3 ubiquitin ligases MuRF1 and MAFbx/atrogin-1. Am J Physiol Endocrinol Metab 2014; 307: E469-484
[34] Karsdal MA, Henriksen K, Leeming DJ, Woodworth T, Vassiliadis E, Bay-Jensen AC. Novel combinations of Post-Translational Modification (PTM) neo-epitopes provide tissue-specific biochemical markers--are they the cause or the consequence of the disease? Clin Biochem 2010; 43: 793-804.
[35] Gezer U, Holdenrieder S. Post-translational histone modifications in circulating nucleosomes as new biomarkers in colorectal cancer. In Vivo 2014; 28: 287-292.
[36] Szabó T, Scherbakov N, Sandek A, Kung T, von Haehling S, Lainscak M, Jankowska EA, Rudovich N, Anker SD, Frystyk J, Flyvbjerg A, Pfeiffer AF, Doehner W. Plasma adiponectin in heart failure with and without cachexia: catabolic signal linking catabolism, symptomatic status, and prognosis. Nutr Metab Cardiovasc Dis 2014; 24: 50-56
[37] Zhang Q, Tang N, Schepmoes AA, Phillips LS, Smith RD, Metz TO. Proteomic profiling of nonenzymatically glycated proteins in human plasma and erythrocyte membranes. J Proteome Res 2008; 7: 2025-2032.
[38] Ang SH, Thevarajah M, Alias Y, Khor SM. Current aspects in hemoglobin A1c detection: a review. Clin Chim Acta 2015; 439: 202-211.
[39] Meng X, Ezzati P, Smolik I, Bernstein CN, Hitchon CA, El-Gabalawy HS. Characterization of autoantigens targeted by anti-citrullinated protein antibodies in vivo: prominent role for epitopes derived from histone 4 proteins. PLoS One 2016; 11: e0165501.
[40] Pruijn GJ, Wiik A, van Venrooij WJ. The use of citrullinated peptides and proteins for the diagnosis of rheumatoid arthritis. Arthritis Res Ther 2010; 12: 203.
[41] Anbalagan M, Huderson B, Murphy L, Rowan BG. Post-translational modifications of nuclear receptors and human disease. Nucl Recept Signal 2012; 10: e001.
[42] Tsai VW, Lin S, Brown DA, Salis A, Breit SN. Anorexia-cachexia and obesity treatment may be two sides of the same coin: role of the TGF-b superfamily cytokine MIC-1/GDF15. Int J Obes (Lond) 2016; 40: 193-197.
[43] Couch ME, Dittus K, Toth MJ, Willis MS, Guttridge DC, George JR, Chang EY, Gourin CG, Der-Torossian H1. Cancer cachexia update in head and neck cancer: Pathophysiology and treatment. Head Neck 2015; 37: 1057-1072.
[44] Deboer, MD. Animal models of anorexia and cachexia. Expert Opin Drug Discov 2009; 4: 1145-1155.
[45] Heimdal K, Sanchez-Guixé M, Aukrust I, Bollerslev J, Bruland O, Jablonski GE, Erichsen AK, Gude E, Koht JA, Erdal S, Fiskerstrand T, Haukanes BI, Boman H, Bjørkhaug L, Tallaksen CM, Knappskog PM, Johansson S. STUB1 mutations in autosomal recessive ataxias-evidence for mutation-specific clinical heterogeneity. Orphanet J Rare Dis 2014; 9: 146.
[46] Fu L, Rab A, Tang Lp, Bebok Z, Rowe SM, Bartoszewski R, Collawn JF. ΔF508 CFTR surface stability is regulated by DAB2 and CHIP-mediated ubiquitination in post-endocytic compartments. PLoS One 2015; 10: e0123131.
[47] Matsumura Y, Sakai J, Skach WR. Endoplasmic reticulum protein quality control is determined by cooperative interactions between Hsp/c70 protein and the CHIP E3 ligase. J Biol Chem 2013; 288: 31069-31079.
[48] Saxena A, Banasavadi-Siddegowda YK, Fan Y, Bhattacharya S, Roy G, Giovannucci DR, Frizzell RA, Wang X. Human heat shock protein 105/110 kDa (Hsp105/110) regulates biogenesis and quality control of misfolded cystic fibrosis transmembrane conductance regulator at multiple levels. J Biol Chem 2012; 287: 19158-19170.
[49] Schisler JC, Rubel CE, Zhang C, Lockyer P, Cyr DM, Patterson C. CHIP protects against cardiac pressure overload through regulation of AMPK. J Clin Invest 2013; 123: 3588-3599.

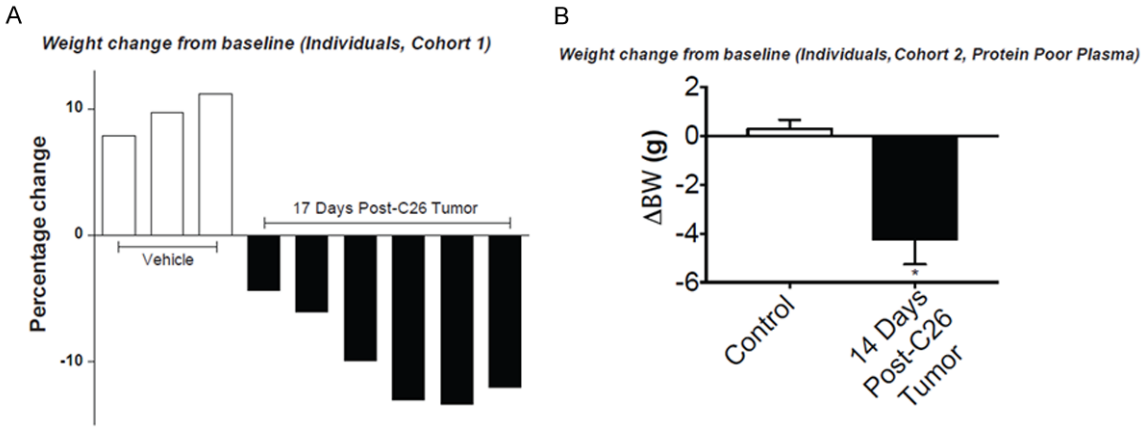

Supplemental Figure 1. Weight changes in control and tumor implanted mice at harvest. A. Weight change as a percent in individual mice as a percentage of their own baseline weights at day 17 in cohort 1. B. Weight change in individual mice in grams compared to their own baseline weights at day 14 in cohort 2. Cohort 1: N=3 vehicle control treated mice; N=6 C26 tumor treated mice. Cohort 2: N=5 vehicle control treated mice; N=5 C26 tumor treated mice. A two-tailed Student's t-test was performed to determine significance. *p<0.05.

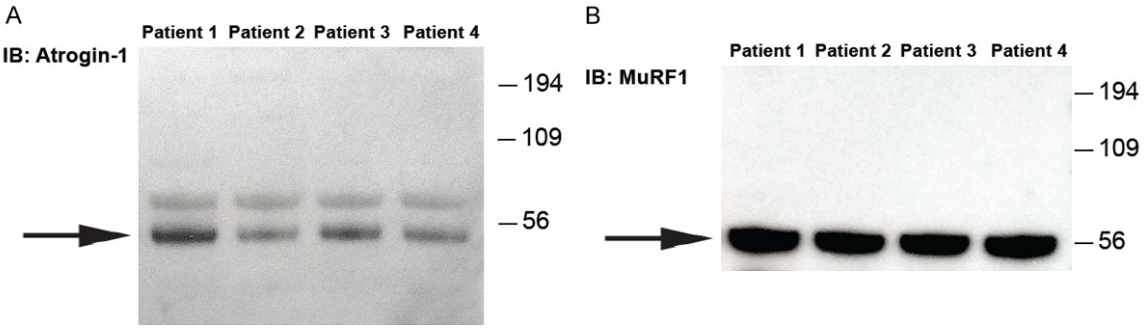

Supplemental Figure 2. Immunoblot analysis of control human plasma samples. Identification of (A). Atrogin-1 or (B). MuRF1 in human plasma. *Black arrow:* Indicates molecular weight of expected protein. N=4 biological replicates.

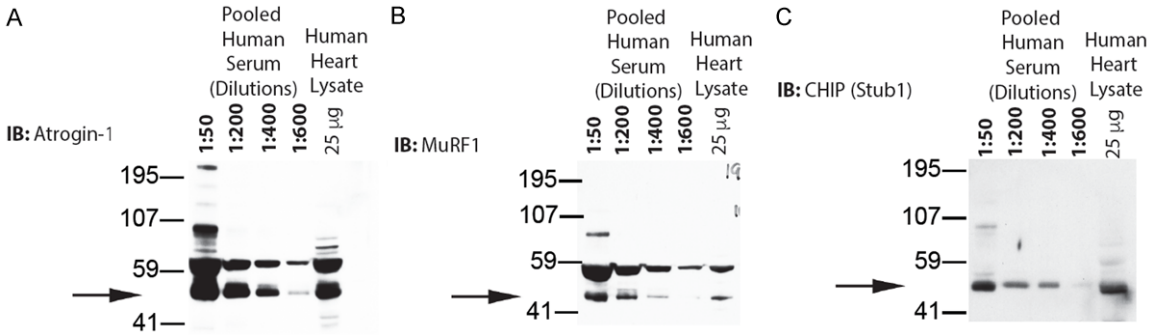

Supplemental Figure 3. Immunoblot analysis of pooled human control serum for (A) Atrogin-1, (B) MuRF1, or (C) CHIP (Stub1). *Black arrow:* Indicates molecular weight of expected protein. Parallel clinical chemistry of the pooled samples can be found in Supplemental Table 1.

Supplemental Table 1. Basic clinical chemistry profile of the human pool-21 used in the present study (Supplemental Figure 3, immunoblot studies on serum dilutions). UNC Hospitals Core (Chemistry) Laboratory anonymous serum pool

Chemistry Analyte	POOL-21 Value	Reference Range	Analyzer Used
Albumin	3.26	3.5-5.0 g/dL	Advia (FSN-1)
Alkaline phosphatase*	146.5	38-126 U/L	Advia (FSN-1)
Alanine Aminotransferase (ALT)*	59.1	Male: 19-72 U/L; Female: 15-48 U/L	Advia (FSN-1)
Amylase	56	30-100	Advia (FSN-1)
Aspartate Aminotransferase (AST)*	77.9	Male: 19-55; Female: 14-38	Advia (FSN-1)
Bilirubin (Conjugated)	0	≤0.1 mg/dL	Advia (FSN-1)
Bilirubin (Unconjugated)	0.47	≤1.2 mg/dL	Advia (FSN-1)
Blood urea nitrogen (BUN)	19.7	7-21 mg/dL	Advia (FSN-1)
C3 (Complement C3)	140.81	88-171 mg/dL	Advia (FSN-1)
C4 (Complement C4)	29.86	15-48 mg/dL	Advia (FSN-1)
Calcium (Ca^{2+})	8.85	8.5-10.2 mg/dL	Advia (FSN-1)
Cholesterol	150.3	<200 mg/dL	Advia (FSN-1)
Creatine Kinase*	228.7	145 U/L	Advia (FSN-1)
Chloride	106.4	98-107 mmol/L	Advia (FSN-1)
Bicarbonate (CO_2)	22.2	22-30 mmol/L	Advia (FSN-1)
Creatine	1.39	Male: 0.8-1.4; Female: 0.7-1.1	Advia (FSN-1)
C-Reactive Protein (hs)*	4.5	1.0-3.0 mg/L	Advia (FSN-1)
Serum Ferritin (Iron)*	67.3	35-165 ug/dL	Advia (FSN-1)
Glucose (Non-fasting)	118.2	65-179 mg/dL	Advia (FSN-1)
HDL Cholesterol	44	40-59 mg/dL	Advia (FSN-1)
Total IgA	254.81	40-400 mg/dL	Advia (FSN-1)
Total IgG	1086.9	600-1700 mg/dL	Advia (FSN-1)
Total IgM	96.76	35-290 mg/dL	Advia (FSN-1)
Potassium (K^+)	4.23	3.5-5.0 mmol/L	Advia (FSN-1)
Lactate Dehydrogenase*	670.4	338-610 U/L	Advia (FSN-1)
Lipase	182	44-232 U/L	Advia (FSN-1)
Magnesium (Mg^{2+})	1.89	1.6-2.2 mg/dL	Advia (FSN-1)
Sodium (Na^+)	138.8	135-145 mmol/dL	Advia (FSN-1)
Rheumatoid Factor	10.2	0.0-15.0 U/ml	Advia (FSN-1)
Total Bilirubin	0.77	≤1.2 mg/dL	Advia (FSN-1)
Total Protein**	6.23	6.6-8.0 g/dL	Advia (FSN-1)
Triglyceride*	150.1	<150 mg/dL	Advia (FSN-1)
Transthyretin (TTR)	21.67	17-34 mg/dL	Advia (FSN-1)
Uric acid	5.1	Male: 4.0-9.0; Female: 3.0-6.5	Advia (FSN-1)
Thyroxine (Total T4)	7.31	5.5-11.0 ug/dL	VitrosECiQ (Eci#1, #3)
Free T4 (FT4)*	1.42	0.71-1.4 ng/dL	VitrosECiQ (Eci#1, #3)
Triiodothyonine (T3)	1.11	1.0-1.7 ng/mL	VitrosECiQ (Eci#1, #3)
Follicle Stimulating Hormone (FSH)	13.4	Male: 1.6-9.7 mIU/mL Female: *Follicular phase*: 1.9-11.6 mIU/mL *Luteal phase*: 1.4-9.6 mIU/mL *Post Menopausal*: 21.5-131.0 mIU/mL	VitrosECiQ (Eci#1, #3)
Leuteinizing Hormone (LH)	6.54	Male: 3.0-10.0 mIU/mL Female: *Follicular phase*: 2.6-12.1 mIU/mL *Luteal phase*: 0.8-15.5 mIU/mL *Post Menopausal*: 13.1-86.5 mIU/mL	VitrosECiQ (Eci#1, #3)
Prolactin	23.6	5-19 ng/mL	VitrosECiQ (Eci#1, #3)
Ferritin*	629	Male: 27-377 ng/mL; Female: 3-151	VitrosECiQ (Eci#1, #3)
Folate	14.4	>2.7 ng/mL	VitrosECiQ (Eci#1, #3)
Prostate Specific Antigen (PSA)	1.76	<4 ng/mL	VitrosECiQ (Eci#1, #3)
CA-125	59.9	0.0-34.9 U/mL	VitrosECiQ (Eci#1, #3)

Carcinoembryonic Antigen (CEA)*	4.23	0-3.0 ng/mL	VitrosECiQ (Eci#1, #3)
Estradiol (E2)	349.4	Male: 5-66pg/mL Female (Postmenopausal): 5-38 pg/mL Female (Ovulating): *Follicular phase* 27-161pg/mL *Periovulatory*: 187-382 pg/mL *Luteal phase*: 33-201 pg/mL	VitrosECiQ (Eci#1, #3)
Progesterone	2.68	Male: <1.00 ng/mL Female: *Follicular phase*: <1.70 ng/mL *Luteal phase*: 1.00-22.40 ng/mL *Post Menopausal*: <1.00 ng/mL	VitrosECiQ (Eci#1, #3)
Cortisol	19.1	*Before 10:00am*: 4.5-22.7 µg/dL *After 5:00pm*: 1.7-14.1 µg/dL *Critical*: <1.5 µg/dL	VitrosECiQ (Eci#1, #3)
Testosterone	74	Male >20 yrs of age: 179-756 ng/dL Female with normal menstrual cycle: 6-77 ng/dL	VitrosECiQ (Eci#1, #3)
Parathyroid Hormone	53.78	12-72 pg/mL	Roche Elecsys (Elecsys #1)
CK-MB	4.82	0-6.0 ng/mL	Roche Elecsys (Elecsys #1)
Troponin T*	0.056	0.000-0.029	Roche Elecsys (Elecsys #1)
NT-proBNP*	3123	Male: 0-177; Female: 0-226	Roche Elecsys (Elecsys #1)
βHCG*	734.7	Non-pregnant: <5 mIU/mL (U/L)	Roche Elecsys (Elecsys #1)

Serum hCG increases with age in non-pregnant women. A cutoff of 14.0 IU/L should be used when interpreting hCG results in women >55 yrs. Pregnancy is unlikely in perimenopausal women 41-55 yrs with an hCG between 5.0 and 14.0 IU/L if serum FSH is >20.0IU/L. *Clin Chem* 2005; 51: 1830-5

WksPreg	Mean	Range	n
4	1110	40-4480	42
5	8050	270-28700	52
6	29700	3700-84900	67
7	58800	9700-120000	62
8	79500	31000-184000	37
9	91500	61200-152000	25
10	71000	22000-143000	12
14	33100	14300-75800	219
15	27500	12300-60300	355
16	21900	8800-54500	163
17	18000	8100-51300	68
18	18400	3900-49400	30
19	20900	3600-56600	14

**Above reference range; **Below reference range.* Analysis for * and ** did not include gender-specific cut-off ranges not applicable to pooled serum.